Tectonics®

RESEARCH ARTICLE
10.1029/2021TC006971

Key Points:

- Apatite thermochronometry record South Vietnam margin exhumation history
- Thermal models are used to test different causes of thermal history
- Regional enhanced cooling and rock uplift between 37 and 30 Ma record early stage rifting

Supporting Information:

Supporting Information may be found in the online version of this article.

Correspondence to:

H. H. Nguyen,
nguyenhuuhiep@humg.edu.vn

Citation:

Huu Nguyen, H., Carter, A., Hoang, L. V., Fox, M., Pham, S. N., & Vinh, H. B. (2022). Evolution of the continental margin of south to central Vietnam and its relationship to opening of the South China Sea (East Vietnam Sea). *Tectonics*, *41*, e2021TC006971. https://doi.org/10.1029/2021TC006971

Received 1 JUL 2021
Accepted 7 JAN 2022

Author Contributions:

Data curation: Hiep Huu Nguyen, Andrew Carter
Formal analysis: Hiep Huu Nguyen, Andrew Carter, Sang Nhu Pham, Hau Bui Vinh
Investigation: Hiep Huu Nguyen
Methodology: Andrew Carter
Project Administration: Hiep Huu Nguyen
Software: Matt Fox
Visualization: Long Van Hoang
Writing – original draft: Hiep Huu Nguyen
Writing – review & editing: Andrew Carter, Long Van Hoang

Evolution of the Continental Margin of South to Central Vietnam and Its Relationship to Opening of the South China Sea (East Vietnam Sea)

Hiep Huu Nguyen[1], Andrew Carter[2], Long Van Hoang[3], Matt Fox[4], Sang Nhu Pham[1], and Hau Bui Vinh[1]

[1]Hanoi University of Mining and Geology, Hanoi, Vietnam, [2]Department of Earth and Planetary Sciences, Birkbeck, University of London, London, UK, [3]Petroleum Exploration & Production Center Vietnam Petroleum Institute, Hanoi, Vietnam, [4]Department of Earth Sciences, UCL, London, UK

Abstract The continental margin of south to central Vietnam is notable for its high elevation plateaus many of which are covered by late Cenozoic basalt flows. It forms the westernmost margin of a wide continental rift of the South China Sea (East Vietnam Sea), and uplift has been considered a result of either rifting or younger intraplate basalt magmatism. To investigate margin development apatite thermochronometry was applied to a dense array of samples collected from across and along the margin of south to central Vietnam. Results, including thermal history models, identified a distinct regional episode of fast cooling between c. 37 and 30 Ma after which cooling rates remained low. The fast cooling coincides with a period of fast extension across the South China Sea (East Sea) region that preceded continental break-up recorded by Oligocene grabens onshore. A thermal model is used test different processes that might influence the inferred cooling including a distinct pulse of exhumation; a decrease in exhumation followed by an associated transient decrease in geothermal gradients and, underplating coincident with rifting. Thermal relaxation following Mesozoic arc magmatism is ruled out as geotherms returned to background rates within 20 Myrs of emplacement, well before the onset of fast cooling. Models support fast cooling attributed to accelerated erosion during early stages of rifting. Some additional heating from either underplating and/or hot mantle upwellings is also possible. No evidence was found to support regional uplift associated with the intraplate magmatism, enhanced monsoon-driven erosion, or seafloor spreading dynamics.

Plain Language Summary This study used apatite thermochronometry to examine the uplift history of South-Central Vietnam to better understand how the elevated landscape formed, and to see if it is connected to the eruption of the widespread basalt flows that cover many of the high elevation plateaus. Results showed a match in the timing between a period of rapid cooling between 37 and 30 million years ago that affected the entire region and a period of fast rifting and extension that ended with continental breakup. To fully understand the cause of cooling thermal models tested different scenarios. Thermal relaxation after magmatism was discounted as it took place well before the period of rapid cooling. Models support fast cooling attributed to accelerated erosion during early stages of rifting. Magmatic underplating associated with rifting might also have produced additional heating but no evidence was found to support regional uplift associated with the basalt magmatism.

1. Introduction

The continental margin of Indochina represents the westernmost margin of the South China Sea, a wide continental rift that in the west is mostly submerged. In the region of south to central Vietnam, the location of this study (Figure 1), the continental margin extends offshore for >100 km before oceanic crust is reached. The extension that led to continental break-up has yet to be fully explained but is known to be related to the subduction of the paleo-Pacific plate, which at the time formed a wide Cretaceous magmatic arc with widespread calc-alkaline magmatism across south to central Vietnam and southern China. Subduction was directed to the northeast beneath southern China and westwards below Vietnam, the eastern margin of the Indochina block (Hall, 2012; Hennig-Breitfeld et al., 2021; Zhu et al., 2004).

Extension is imprinted on the landscape and geology of Vietnam but to what extent is not yet clear. It also remains uncertain as to when surface uplift took place. Was uplift staggered over a long time or did it occur within a short

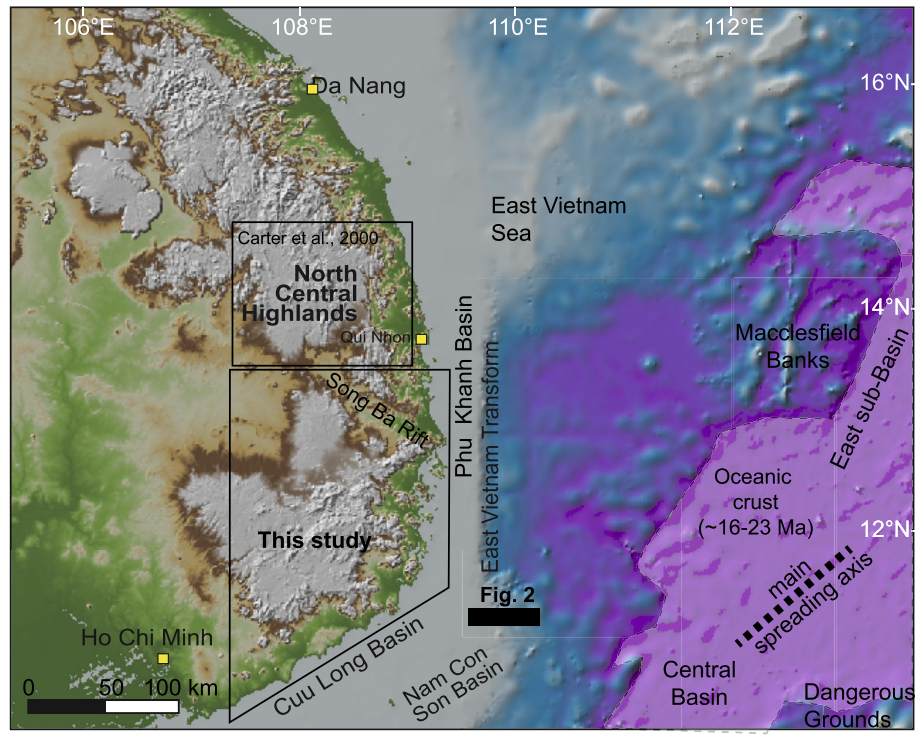

Figure 1. Location of the study area that compliments an earlier study of the Kontum region (Carter et al., 2000).

episode? Stratigraphic evidence provides some constraints. In south-central Vietnam many of the high plateaus, with typical elevations between 500 and 1500 m a.s.l. (Figure 1), are covered by basalt flows (mainly tholeiites) the majority of which were erupted between the late Miocene to Quaternary (An et al., 2017; Hoang et al., 2013). Eruptions were often from extensional faults or small axial rifts that formed previously during extrusion and opening of the South China Sea (Flower et al., 1998; Hoang & Flower, 1998). Rangin et al. (1995) recognized that many of the normal faults associated with these basalts were reactivated N 160°E to N-S right-lateral faults. However, the timing of extension across this margin is not well defined. A common view is that extension involved uplift of the rift shoulders and that this drove widespread erosion from the latest Cretaceous-early Paleocene (Andersen et al., 2005; Lee et al., 2001; Lee & Watkins, 1998; Matthews et al., 1997; Pubellier et al., 2005; Roques et al., 1997). However, onshore, there are no geological constraints at outcrop to confirm this. Basalt flows can be seen to drape over Precambrian to Proterozoic crystalline and metamorphic basement rocks and in some places Jurassic to Cretaceous and late Neogene sedimentary and magmatic rocks, but the temporal gap between the youngest rocks is large, for example, exhumed Cretaceous granites, and their basalt cover spans 80–90 Myrs. Offshore constrains are little better. In southern Vietnam the Cuu Long and Nam Con Som rift basins record a c. 50 Myr gap between the Eocene clastic sediments that were deposited on exhumed Cretaceous granites and older rocks (Fyhn, Boldreel, & Nielsen, 2009).

As the deformation and tectonic evolution of the continental margin of south-central Vietnam and its relationship to the opening of the South China Sea is poorly resolved we conducted a thermochronometry study based on apatite U-Th-He and fission track (FT) data using rock samples collected from across the continental margin. The utility of this approach is demonstrated by previous work on the Kontum region (Figure 1) of central Vietnam (Carter et al., 2000) that identified a late Miocene increase in exhumation rates across the central margin contemporaneous with increased sedimentation in the adjacent Phu Khan marine basin. It was unclear if this phase of exhumation was caused by surface uplift of the continental margin and base level change associated with breakup of the southwest subbasin of the South China Sea (Fyhn, Boldreel, & Nielsen, 2009, Fyhn, Nielsen, et al., 2009; Savva et al., 2014) and/or switching between rifting and left-lateral transtension along the East Vietnam Boundary Fault Zone (Figure 1). An alternative explanation is that late Cenozoic magmatism had a local influence on rock uplift (Carter et al., 2000). Finally, work by Clift et al. (2015) proposed that basin subsidence histories may have been affected by increased loading associated with monsoon intensification driving faster sediment delivery

to offshore basins and therefore enhanced exhumation could be due to erosional unloading related to changes in monsoon intensity.

2. Geological Background

During the Cretaceous eastern Indochina was part of a wide Andean type continental margin. Radiometric dates record calc-alkaline magmatism between 118 and 87 Ma (Hennig-Breitfield et al., 2021; Shellnutt et al., 2013; Thuy et al., 2004). The end of this magmatism coincided with docking of the Luconia-Dangerous Ground block with Indochina, and with South China moving to the southeast to become part of the South Asia margin (Fyhn, Boldreel, & Nielsen, 2009; Hall, 2012). The combination of these changes likely drove the early rifting of the Proto-South China Sea, in either a back-arc setting to the East Asian margin or within a slab-pull environment linked to microcontinent detachment along Northern Borneo (Doust & Sumner, 2007).

Spreading in the South China Sea started at c. 32 Ma (Barckhausen et al., 2014) and affected the continental margins of both Indochina and SE China. Pre-spreading extension of the continental lithosphere produced more or less E-W oriented normal faults across SE China and the South Vietnam margin, although in the Cu Long basin the orientation is closer to SW-NE (Schmidt et al., 2019). With the onset of ocean spreading, the orientation of new faults moved to NE-SW reflecting the progression of spreading to the southwest (Savva et al., 2014). A ridge jump at 25 Ma relocated spreading to a southwestern subbasin until spreading ended at 15 Ma (Li et al., 2014), when the subduction zone became blocked by collision with continental fragments (northern part of Palawan and/or a part of the Dangerous Grounds).

It is widely assumed that Late Cretaceous to Early Paleocene early stage extension drove uplift of the rift shoulders and was followed by widespread erosion and peneplanation (Taylor & Hayes, 1983), but this is based on offshore seismic interpretations of poorly dated early syn-rift sediments. The imprint of extension and rifting on the south-central Vietnam continental margin is different from the SE China margin due to a combination of reactivation of inherited structures (mainly Indosinian) and the local influence of tectonic extrusion driven by India-Eurasia collision (Fyhn, Boldreel, & Nielsen, 2009). Although the amount of left-lateral extrusion is debated (Searle et al., 2010) the position and orientation of Indochina must have changed throughout the period of South China Sea opening, and any change would have affected the regional stress field. Four phases of late Mesozoic-Cenozoic deformation are recognized in Vietnam; (a) E-W compression, N-S extension, (b) NNW-SSE compression, ENE-WSW Extension, (c) N-S compression, E-W extension, and (d) NNE-SSW compression, ESE-WNW extension (Nguyen & Hoai, 2019).

2.1. Records From Offshore Basins

Extension and rifting led to the formation of the Phu Khanh and Cuu Long basins (Figure 1). The Phu Khanh Basin was controlled by the N-S striking East Vietnam Boundary Fault, considered a continuation of the Red River Shear Zone, as well as NE-SW directed normal faults (Fyhn, Boldreel, & Nielsen, 2009). Further south the Cuu Long Basin is bounded by NE-SW to E-W striking normal faults (Schmidt et al., 2019). The sedimentary archives of these basins reflect onshore erosion.

2.2. Phu Khanh Basin

This mainly deep-water basin is situated at the base of the continental slope off central Vietnam and is separated from the mainland by the East Vietnam Boundary Fault (Figure 1; Fyhn, Nielsen, et al., 2009). The basin history records two major rifting events (Lee & Watkins, 1998; Savva et al., 2014). Syn-Rift I in the Palaeogene was accompanied by the deposition of clastic and lacustrine sediments. Syn-Rift II is associated with the opening of the South China Sea and from the end of the Oligocene involved mainly marine sedimentation. A distinct unconformity marks the Paleogene-Neogene boundary (Fyhn, Nielsen, et al., 2009) across which rifting decreased significantly. Post-rift sediments include upper Miocene-Pliocene turbidite fans interpreted as the product of high rates of onshore erosion (Figure 2).

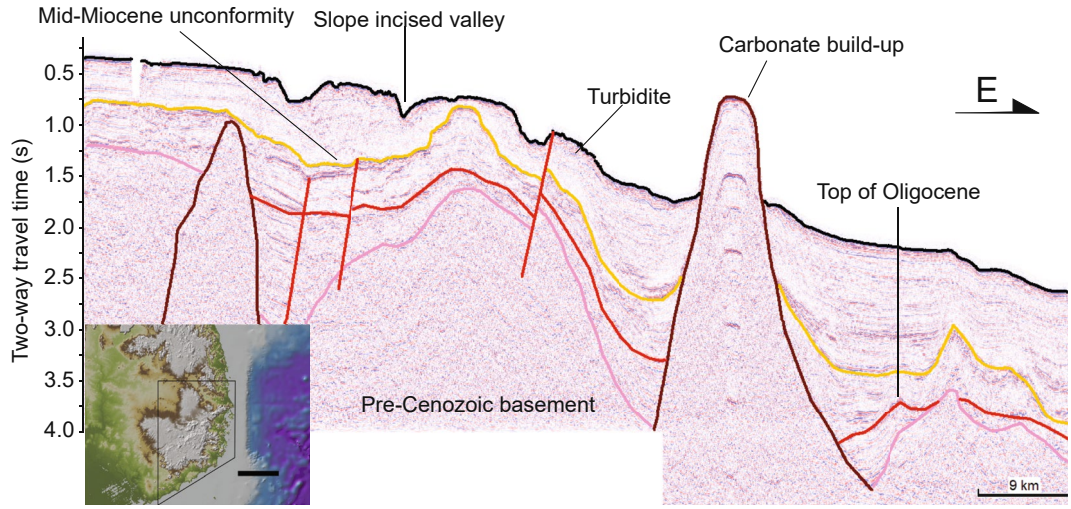

Figure 2. Seismic profile across the continental margin adjacent to the study area (Vietnam Petroleum Institute). A distinct Oligocene unconformity records basin inversion and a mid-Miocene unconformity records the end of rifting after which sediment supply increased leading to progradation and slope mass transport deposits.

2.3. Cuu Long Basin

This basin is located offshore southeast Vietnam (Figure 1) across the continental shelf and was formed by rifting during the Late Eocene-Early Oligocene (Schmidt et al., 2019). The basin contains up to 8 km of mainly clastic sediments deposited between the Eocene to Quaternary (Morley et al., 2019). A narrow valley developed during the first (syn-rift) phase of extension, and in the basin axial zone rapid subsidence took place in the late Oligocene. While extensional deformation extended into the Miocene, a distinct unconformity at ~27 Ma marks inversion and a transition to post-rift sag. The main phase of post-rift thermal sag took place after 23 Ma (Morley et al., 2019).

In the Early Miocene, a new phase of seafloor spreading was accompanied by a period of sea level rise. This caused a marine transgression in all of the basins along the western edge of the South China Sea (Lee, et al., 2001) leading to the formation of carbonate and coral reefs (Fyhn, Boldreel, & Nielsen, 2009). Later post rift subsidence formed a broader shallow sag basin with clastic sedimentation. Our low-temperature thermochronometry results should show which parts of the continental margin experienced the enhanced erosion that drove the clastic sedimentation recorded in the offshore basins.

3. Methodology

The partial retention zone (c. 80–40°C) of the (U-Th-Sm)/He (AHe) and partial annealing zone (c. 130–60°C) of the apatite fission track (AFT) methods are well placed to provide constraints on timing, rate, and magnitude of bedrock exhumation in the uppermost crust (Lisker et al., 2009). For this study a primary goal is to use apatite thermochronometry to detect when rock uplift and exhumation accelerated in response to either surface uplift and/or denudation. Mapping the pattern of exhumation in relation to the extended continental margin will allow assessment of the impact of extension on the continental margin of southern Vietnam. This aim guided our bedrock sampling strategy that comprised a series of north to south, coast to interior transects across the study area, spanning the local relief. Studies of rift and passive margin erosion patterns based on apatite fission track data (Wildman et al., 2019) have shown that the amount of erosion is generally greatest along the coastal areas and decreases inland. This is mainly due to isostatic unloading: as a rift escarpment migrates inland, rock uplift rates remain high close to the margin leading to higher exhumation rates and younger ages. Variations in erosion caused by local geomorphic conditions and geology such as reactivation of inherited faults and magmatic underplating add noise to this dominant trend.

In total 67 samples were collected of which 42 (Figure 3) produced good quality apatite suitable for analysis. Each sample weighed between 2 and 5 kg and were mainly granites as early sampling found that other rock types

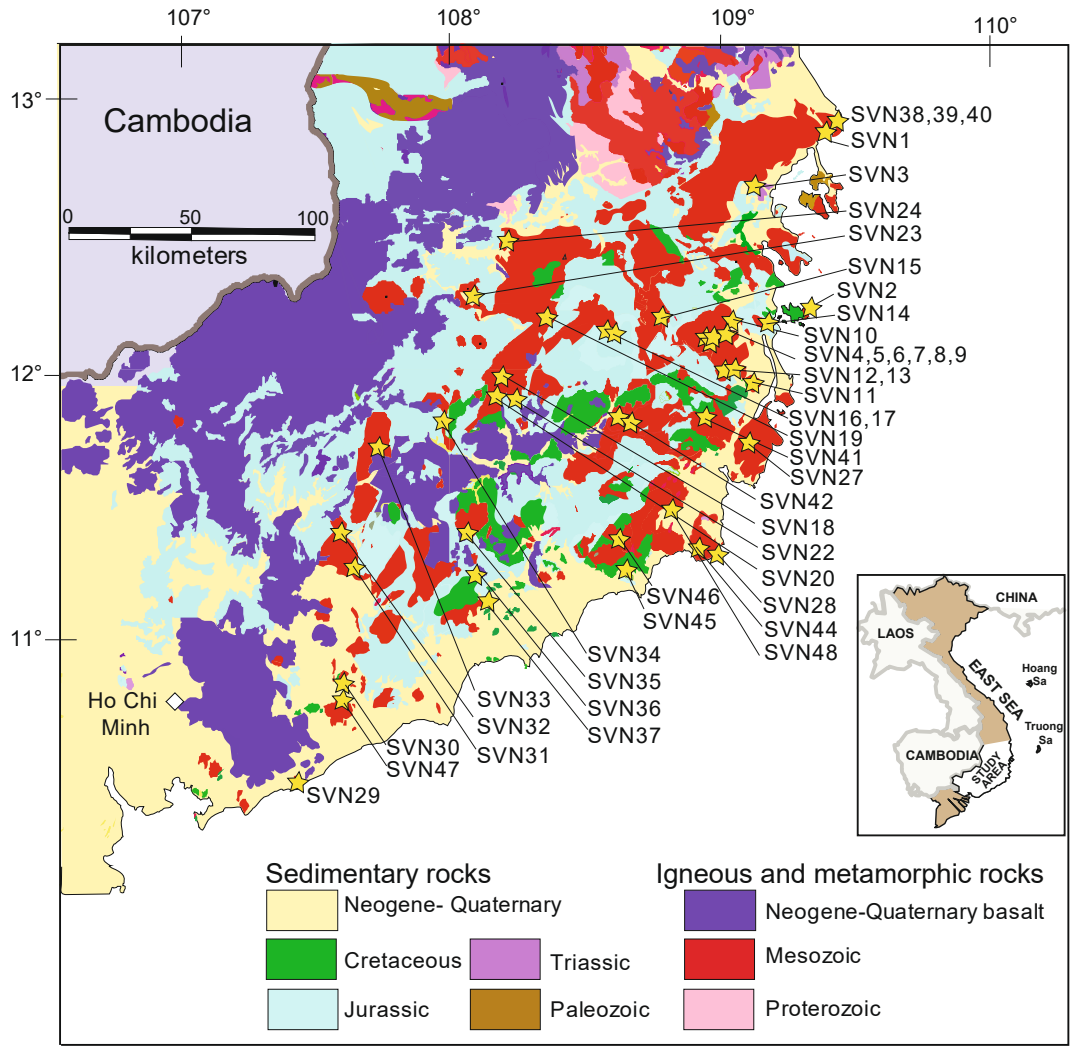

Figure 3. Sample locations and regional geology modified from Luong et al. (1988).

contained little, if any, apatite. Table S1 in Supporting Information S1 details sample locations. All thermochronometry analyses were conducted at the London Geochronology Centre. Fission track analyses used conventional neutron irradiation procedures based on the external detector method and zeta calibration approach (Hurford & Green, 1983). Apatites were mounted, polished, and etched in 5N nitric acid 20°C for 20 s. Track length measurements were used to constrain sample cooling rate, and grain bulk composition was monitored using etch pit length (DPAR) measured parallel to the crystallographic c-axis (Donelick, 1993) (U-Th-Sm)/He analyses typically involved between 4 and 6 replicates. Apatite grains were placed in platinum tubes and outgassed using a 25 W, 808 nm diode laser and ^{4}He measured on a Balzers quadrupole mass spectrometer. Following apatite dissolution and spiking U, Th, and Sm concentrations were measured on an Agilent 7700x ICP-MS. Further details on the analytical protocols can be found in Supporting Information S1.

4. Results

4.1. Low-Temperature Thermochronometry

Apatite (U-Th-Sm)/He analysis was performed on 18 representative samples from across the elevation range (Table S2 in Supporting Information S1). These typically show age dispersion between individual replicates, some of which can be explained by variations in grain size, accumulated radiation damage, and apatite chemical composition (Figure S1 in Supporting Information S1). Such factors can affect helium diffusion kinetics and

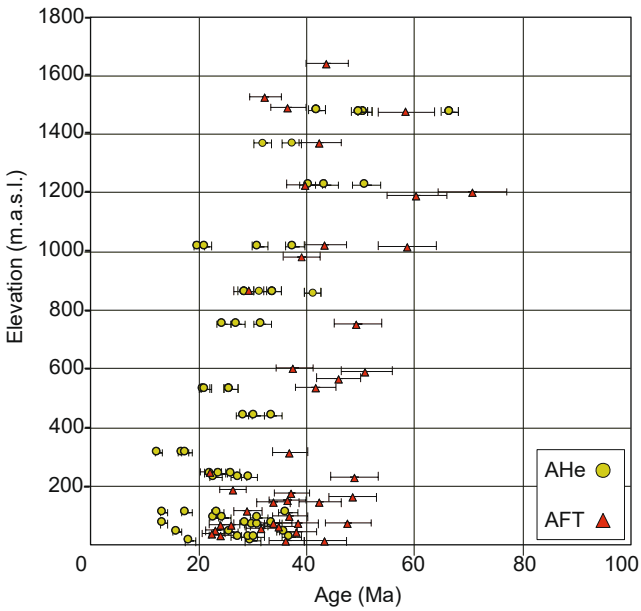

Figure 4. Plot comparing apatite fission track and AHe (corrected) replicate ages against sample elevation. Because the samples are from a range of locations with different exhumation rate histories, the slope of this relationship will not approximate the exhumation rate. In addition, elevation varies with distance from the coast and so this variability also masks obvious trends. Error bars are 1s.

produce a range of (U-Th)/He dates from a single rock. However, spurious ages can also arise from alpha particle implantation from external sources, U-Th rich inclusions, inaccurate grain size measurement and alpha ejection correction, problematic outgassing, incomplete grain dissolution, and sample handling. Outlier ages were only rejected where there was clear evidence of experimental issues.

AFT analysis was carried out on 47 samples of which 44 yielded good quality age data (Table S3 in Supporting Information S1). By contract, track length data was affected by low spontaneous track densities and only 11 samples yielded sufficient track lengths for modeling. Sample central ages range from 70 ± 5 to 22 ± 3 Ma, with a weighted average of 41 Ma. Apatite etch pit lengths measured parallel to the grain c-axis (DPAR), a proxy for grain bulk composition ranges from 1.7 to 3.8 µm. If cooling rates were low DPAR and AFT age would be expected to correlate, due to a compositional influence on FT annealing. As there is no correlation this implies cooling rates were not slow, borne out by FT track length data (samples with >50 measurements) that show unimodal distributions and long mean lengths between 13.5 and 14.2 µm (n = 16). Furthermore, a comparison between AHe ages and effective uranium (eU) values and grain radius, based on a spherical geometry, revealed no trends to support slow cooling (Figure S1 in Supporting Information S1). If this were the case single AHe ages should correlate with eU (proxy for radiation damage; Flowers et al., 2009) Likewise, larger grains, with a slightly higher closure temperature, would be appreciably older than smaller grains if cooling was slow.

Figure 4 plots all replicate AHe ages and AFT central ages against sample elevation. Most ages fall between 20 and 60 Ma, irrespective of sample elevation, and implies a phase of regional uplift. There is no well-developed age trend between coastal areas and furthest points inland as would be expected from a conventional passive margin whereby the youngest ages would be confined to the coastal areas and oldest ages restricted to the highest elevations inland. Within the data set, AHe ages tend to increase with elevation but this is less well developed in the AFT data. A clearer signal is detected in Figure 5 that shows ages plotted for a suite of samples collected across a 1421 m elevation range within a 92 Ma granite, located close to Nha Trang on the coast. Proximity to the coast means that the data are more likely to record a primary signal of rock uplift and erosion: points further from the coast will be less sensitive to a geomorphic response to rock uplift. In other words, any delay between uplift and erosion will depend on geomorphic processes, which may take longer to respond to changes in tectonics further from the base level (sea-level). The plot shows exhumation rates accelerated after 40–50 Ma based on the changing slopes of the age-elevation relationship.

4.2. Thermal History Models

To constrain rock uplift history, the thermal histories of representative samples, with sufficient track length measurements, were obtained using the QTQt software of Gallagher (2012). This is based on a Bayesian transdimensional approach to data inversion to extract probable thermal histories. Model outputs are accepted thermal history models that can be combined to give a mean thermal history model weighted by the posterior probability of each individual thermal history with 95% credible intervals that provide a measure of uncertainty. Model runs allowed the temperature offset to vary over time and data were predicted using the annealing and diffusion models Ketcham et al. (2007) and Gautheron et al. (2009). Granite emplacement age was the only time-temperature constraint used in the inversion based on our own zircon U-Pb analyses or published ages (Hennig-Breitfield et al., 2021; Shellnutt et al., 2013).

Results from the multisample vertical profile inversion shown in Figure 5 are presented in Figure 6. Models produce a reasonable fit to the data although some AHe ages are underpredicted. For the low elevation data underprediction, could be due to a recent increase in cooling such that the amount of rock uplift and exhumation is insufficient to provide a clear signal in the AHe data. However, thermal history models of low elevation

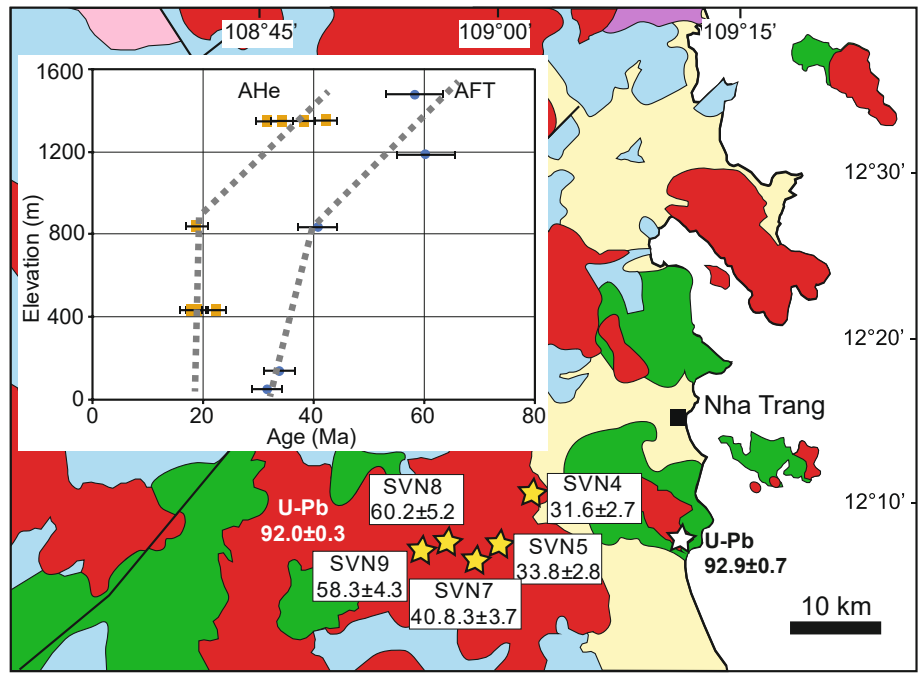

Figure 5. Apatite fission track and AHe (corrected) ages for a suite of samples collected across a 1421 m elevation range within a 92 Ma granite. Ages above 800 m record slower exhumation than samples at lower elevation. Key to geological units given in Figure 3.

samples with the youngest AHe ages from across the study area (S2) show no significant departure from the post 30 Ma cooling path in Figure 6. Likewise models of high elevation samples from across the study area are consistent (residence at crustal temperatures <60°C since 50–60 Ma) with the thermal history model in Figure 6. The models suggest the region experienced a multistage thermal history that involved accelerated cooling between 60 and 50 Ma, minor reheating between 50 and 35 Ma, and accelerated cooling between ~37 and 30 Ma followed by constant cooling to the present. The early phases of cooling are not well constrained as the oldest tracks do not extend to the middle Cretaceous, hence the thermal history between 90 Ma and about 50 Ma is largely unconstrained, driven by the requirement to start at the time of granite emplacement. Resolution increases through time as shown by the difference between the credible intervals for specific samples. The reheating stage of the history from 50 to 37 Ma is relatively well resolved. From 37 Ma, however, resolution increases and the accelerated cooling between 37 and 30 Ma is well constrained and consistent with the regional age-elevation data plotted in Figure 5. These two stages require average offset temperatures (differences between lowest and highest elevation samples) to rise to up to 80°C equivalent to a geothermal gradient of ~57°C/km, but then temperature offsets decrease through time. This decrease in geothermal gradient through time is partly required by the fact that both high and low elevation samples must reach similar temperatures at the surface. However, the ages are sensitive to times as recent as 20 Ma and therefore, the change in geothermal gradient is likely to be robust and not an artifact.

5. Discussion

Dense sampling across the study area, extending from the coast to up to 75 km inland yielded 42 AFT ages and 77 AHe replicate single grain ages distributed across an elevation range of 1,524 m. Ages do not increase from the coast to inland as would be expected from a typical rifted margin where there is limited erosion landward of an escarpment (Gallagher & Brown, 1997). The majority of sample ages cluster between 20 and 50 Ma, independent of elevation, consistent with regional block uplift. Although some of the highest elevation data show a relationship between age and elevation reflecting an earlier exhumation history, most of the data below 800 m record similar ages indicative of faster cooling. This contrast in cooling rates is best seen in data from a suite of samples collected across a 1.4 km vertical section of a 92 Ma granite (Figure 5) that captures the regional thermal

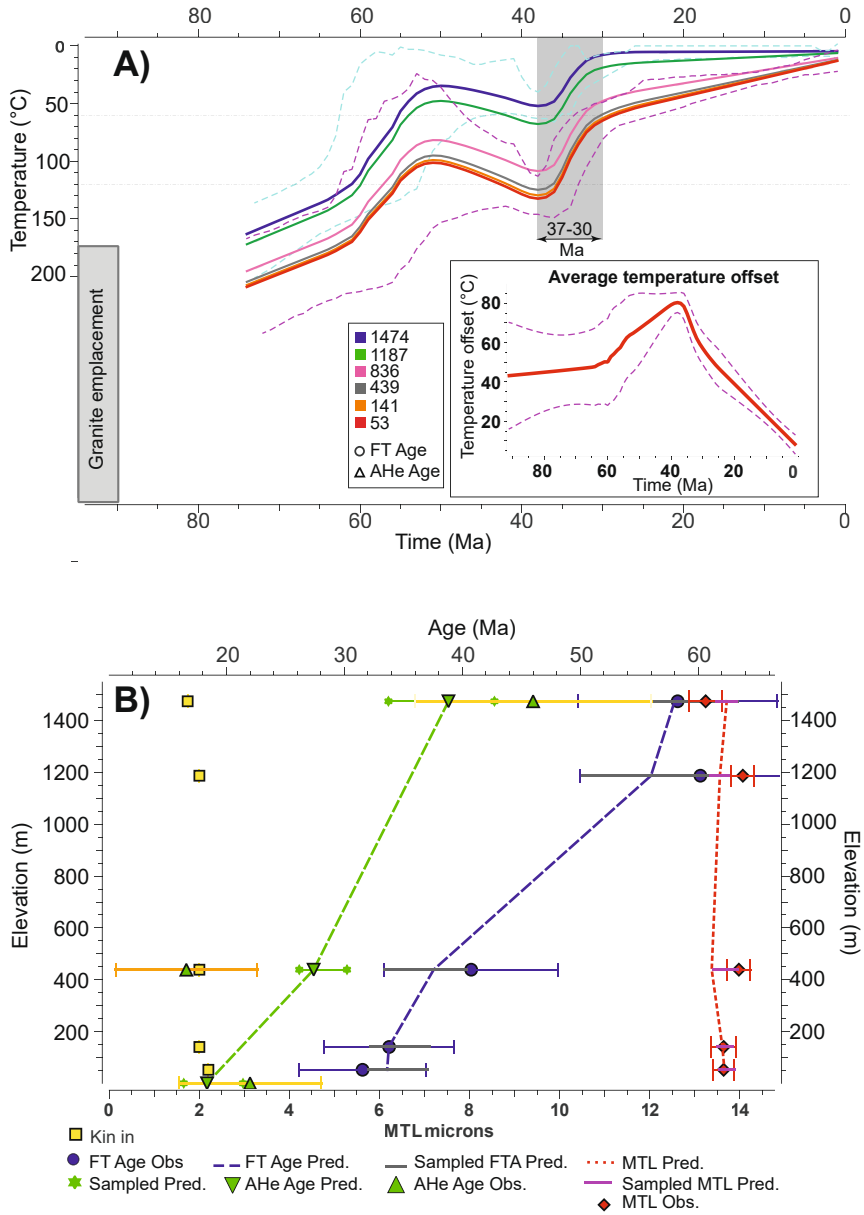

Figure 6. Thermal history model of the vertical profile shown in Figure 5. Dark column denotes the circa 37–30 Ma onset of fast cooling recorded by the best-fit models. Solid lines are best fit models. The credible intervals (dashed lines) are shown only for the lowermost and uppermost samples. Plot 6b shows how well the models fit the measured data by plotting the predicted and observed values as a function of elevation. Error bars include the mean 95% credible range for the predictions from all thermal history models accepted during the post-burning MCMC sampling.

history. QTQt thermal history models (Figure 6) show a multistage history with reheating between ~50 and 37 Ma, and a well-resolved accelerated cooling between 37 and 30 Ma followed by uninterrupted slower cooling to the present. Differences in temperature between the lowermost and uppermost samples between 60 and 30 Ma require a high geothermal gradient (c. 57°C/km) that when applied to the accelerated cooling between ~37 and 30 Ma would crudely translate to about 1,500 m of rock uplift and exhumation. This regional thermal history raises several questions: (a) What caused the interval of reheating between 50 and 37 Ma? (b) What caused the interval of accelerated cooling between 37 and 30 Ma and was this period related to the generation of present-day topography? (c) Are there any connections between changes in cooling rate, the opening of the South China Sea (East Vietnam Sea), and sedimentation in the marine basins?

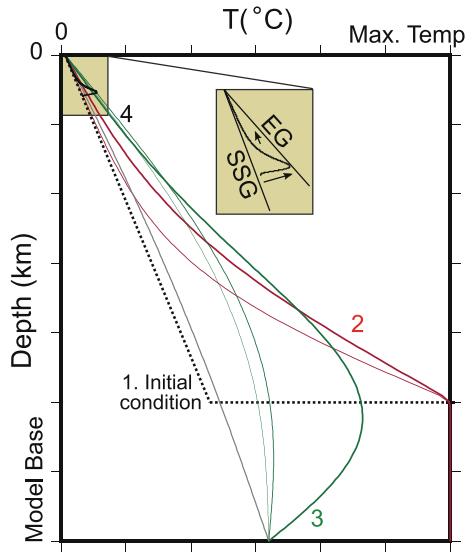

Figure 7. A simple 1D model is used to assess the effects of heating at depth on the time-temperature paths experienced by thermochronometry samples. In this cartoon, the initial condition is shown by the dotted line. Here, temperature increases linearly with depth and then there is an increase in temperature associated with the magma (1). Temperatures remain high to simulate an active magma chamber. This leads to heating above the magma chamber (2). After a set amount of time, temperatures at the base of the model return to a temperature defined by the initial geothermal gradient (3). Temperatures remain high across the upper part of the model (4). Over time temperature return to a steady state thermal model determined by the boundary conditions and exhumation rate. The inset shows the evolution of temperature a material point experiences as it is exhumed toward the surface. Initially there is heating to the elevation geotherm and then temperatures decrease to the steady state geotherm.

In order to address these questions, we require a thermal model that relates cooling histories of rocks to changes in exhumation rate and the thermal structure of the crust. Using this thermal model we can test different factors that might influence the inferred cooling. In the next section, we first highlight that the elevated heating from arc magmatism and emplacement of the sampled granites is a transient feature that does not persist beyond about 20 Myrs. Therefore our resolved changes in cooling since about 50 Ma are related to other processes. We highlight three different processes that predict similar cooling histories: a distinct pulse of exhumation; a decrease in exhumation followed by an associated transient decrease in geothermal gradients; and, recent underplating coincident with rifting but unrelated to arc magmatism and recent basaltic magmatism.

We use a simple 1D transient thermal model to explore these processes. The model solves the heat transport equation with Dirichlet boundary conditions at surface and lower crustal temperatures, tracking material points through the evolving thermal field to provide time-temperature paths. Numerically, the model uses finite differences in space and the Crank-Nicolson method for temporal integration (see Fox & Carter, 2020). The thermal model is 35 km thick, used boundary conditions set at 15°C at the surface and 800°C at the base to give an unperturbed geothermal gradient of 22°C/km as this is about the average geothermal gradient predicted by the QTQt models over the last 40 Ma. A thermal diffusivity of 25 km^2/Ma is used for all models. The time-step length is set to 1×10^{-3} Myr and the vertical resolution is 0.2318 km. The initial condition is modified to reflect the emplacement of magmas at different depths. Exhumation rate histories are also modified to explore the different scenarios.

5.1. Relationship Between Cooling and Exhumation

5.1.1. The Influence of Magmatic Heating During Emplacement

As a former magmatic arc the study area would have experienced increased heating and elevated geothermal gradients followed by post-magmatic thermal relaxation. A fundamental question is whether this impacted the low-temperature thermochronology data. Murray et al. (2018) investigated this question using 1D and 3D models in which heat diffused from a magmatic emplacement and rocks were advected toward the surface. They were able to show that large midcrustal plutons, emplaced at depths between 10 and 15 km, can reset low-temperature thermochronometers in the upper crust. This is not surprising, but of importance to this study is the question of how long such thermal effects persisted following magma emplacement? There is at least a 40 Myr gap between granite ages and the earliest cooling constrained by the apatite data. Could this early stage cooling be a consequence of post magmatic thermal relaxation? To explore this we used the same approach as Murray et al. (2018) to assess the effects of heating at depth on the time-temperature paths experienced by thermochronometry samples. The cartoon in Figure 7 shows the basic evolution of the model. Heating can lead to increased geothermal gradients at all depths. Samples that are exhuming will experience this heating and subsequent cooling. The exact heating and cooling rates will depend on the duration of heating, the exhumation rate, the depth of heating and the samples and the thermal diffusivity of the crust (Murray et al., 2018).

Figure 8 shows the results of a numerical model designed to simulate high temperature at the start of the model. Here, temperatures are high during the first 2 Myrs of the model run from 8 to 12 km depth. This heats a large section of the crust. After this initialization period, heat is lost through diffusion and temperatures rapidly return to a steady state solution. It is important to note that the steady state solution shows slightly higher geothermal gradients than the initial condition due to the advection of heat driven by erosion which is constant at 0.1 km/Myr. The rocks that are at the surface at the end of the model are tracked along the red curve. This is highlighted in Figure 8b and shows the rapid cooling following emplacement. For reference, a thermal history is shown in which there is no heating at the start of the model. Only the high temperature $^{40}Ar/^{39}Ar$ in hornblende and muscovite

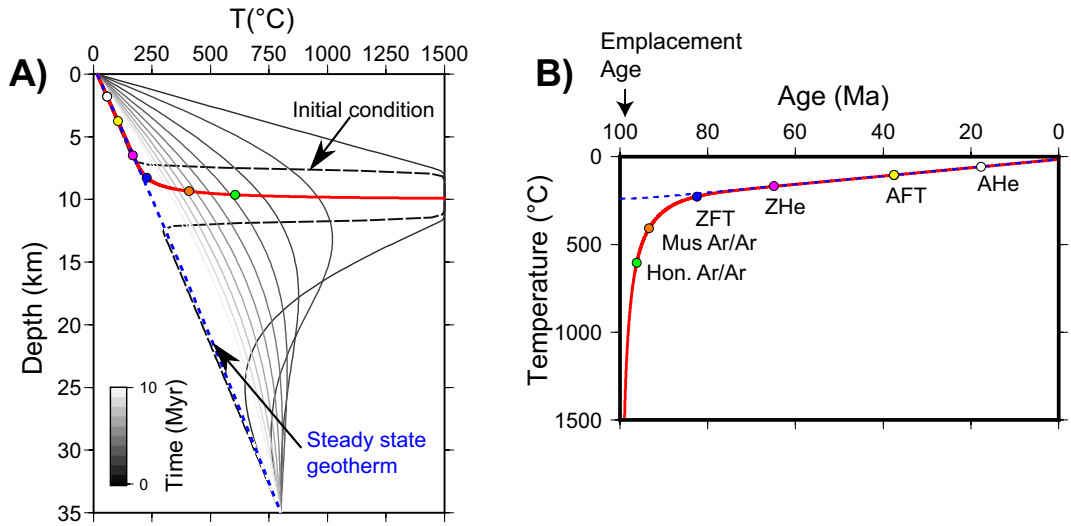

Figure 8. The duration of heating associated with magma intrusion. A magma intrusion is simulated between 8 and 12 km depth. Temperatures remain high for 2 million years before the basal boundary condition at 35 km is forced to 800C. The exhumation rate remains constant at 0.1 km/Ma. The gray curves show the evolving thermal model over the first 10 million years of the simulated history. After approximately 20 million years the steady state solution is reached and temperature as a function of depth remains constant. The red line shows the temperature-depth path rocks that reach the surface took. The circles show the closure temperatures and depths evaluated using Dodson's approximation. (b) This same path can be plotted as a function of temperature and age. This highlights the rapid cooling from temperatures of 1,500°C to temperatures of about 250°C over the first 20 million years of the simulated history. For reference, a time-temperature path from a thermal model with no heating is shown by the blue dashed line.

thermochronometric systems would be influenced by this heating event. The other thermochronometers would not be sensitive to this thermal event and therefore, we can begin the subsequent models at 40 Ma.

Next, we consider two other processes that may produce similar, high rates of cooling over the same sort of time interval: (a) relaxation of geothermal gradient following the cessation of exhumation and, (b) cooling following a pulse of heating associated with emplacement of underplating material below the lower crust associated with the rifting.

5.1.2. Changes in Exhumation Rate

We use a reference scenario in which the cooling is interpreted in terms of exhumation (Figure 9). In this scenario, a pulse of exhumation with rates of 0.6 km/Ma is simulated between 37 and 30 Ma and the background rate is set to 0.02 km/Ma (consistent with Quaternary cosmogenic erosion rates measured in a river catchment to the north of the study area by Jonell et al., 2017). This leads to relatively fast cooling over this time interval recreating the accelerated cooling between 37 and 30 Ma. However, the peak in cooling rate is at 30 Ma and there is just a small change in the geothermal gradient. This is in contrast with the results of the QTQt model that highlights large changes in the geothermal gradient through time. It is important to note that we are highlighting the geothermal gradient at the changing depth of the synthetic sample as it is exhumed. This is to be consistent with the temperature offset resolved by QTQt. In addition, it is not clear how exhumation rates might change so abruptly given the gradual changes in surface processes expected following changes in rock uplift.

A second scenario is simulated in which a pulse of exhumation that began at 40 Ma at rates of 0.75 km/Ma and then decreased exponentially from 37 Ma to the present to a background rate of 0.01 km/Ma (Figure 9). This exhumation rate history approximates a geomorphic response to rock uplift in which erosion rates are high during rock uplift and then decay after the cessation of active rock uplift. High rock uplift rates elevate the geothermal gradient due to the advection of heat. As exhumation rates decrease, the geothermal gradients relax but rocks continue to exhume. Importantly, the peak in cooling rate actually postdates the phase of active rock uplift and therefore the phase of rapid cooling resolved by the thermochronometric data may be the result of an earlier phase of active rock uplift. Although this scenario modifies the geothermal gradient due to heat advection, the

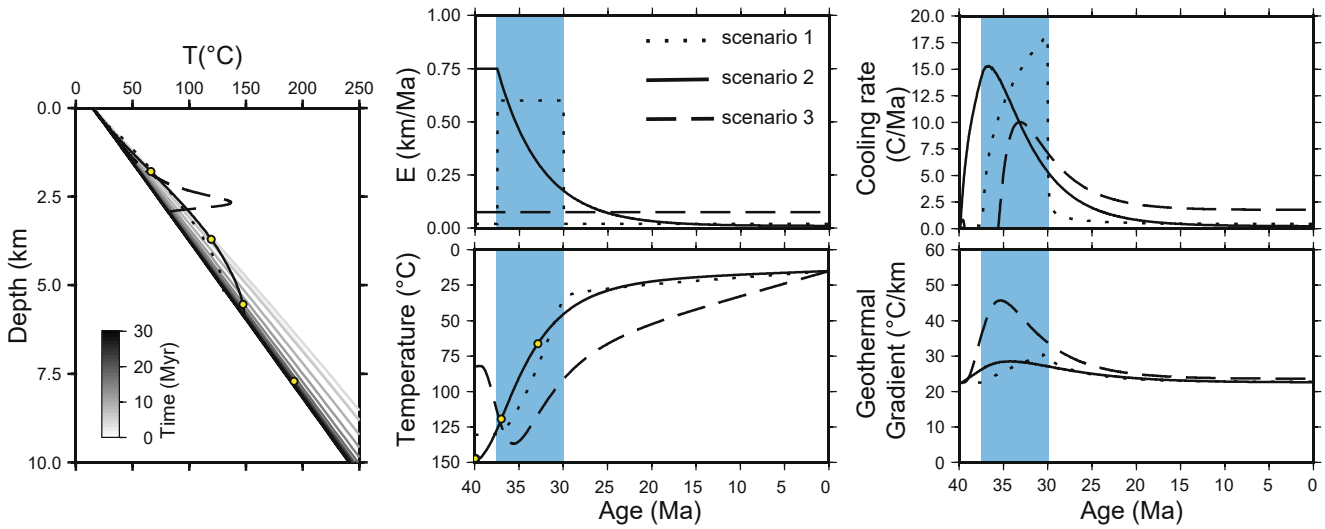

Figure 9. Thermal models for three different thermokinematic scenarios used to predict the evolving thermal field: Dotted line (scenario 1) is where the cooling was interpreted in terms of exhumation, with rates of 0.6 km/Ma between 37.5 and 30 Ma and a background rate of 0.02 km/Ma. The solid line (scenario 2) approximates a geomorphic response to rock uplift where exhumation began at 40 Ma at rates of 0.75 km/Ma but then decreased exponentially from 37 Ma to the present background rate of 0.01 km/Ma. The dashed line (scenario 3) represents a pulse of heating associated with emplacement of underplating material below the lower crust and highlights how a pulse of heating within the lower crust could also produce a pulse of cooling. Blue shaded areas show the interval of rapid cooling indicated by QTQt models (Figure 6). All curves show increased cooling rates between about 35 and 25 Ma. Scenario 3 also shows a reheating event.

magnitude of the change in geothermal gradient is not as large as inferred using QTQt. As with the first scenario, geothermal gradients decrease following the phase of fast exhumation.

5.1.3. Changes in Boundary Conditions

A third scenario simulates the emplacement of underplating material below the lower crust (Figure 9). In seismic sections further to the north in the South China Sea, lower-crust high-velocity anomalies have been observed and related to magmatic underplating at depths of about 25–30 km (Li et al., 2020). In this model a pulse of heating is set to 1,500°C between depths of 25 and 35 km from 40 to 38 Ma and this simulates a change in temperature at the base of the crust associated with rifting. Such depths and temperatures are not unrealistic as the geochemistry of local Cenozoic calc alkali magmatism indicates a hotter than normal shallow asthenosphere (Hoang et al., 2013) and the lithosphere in this study area is some 20–30 km thinner than Northern Vietnam (Vu et al., 2021), presumably in part due to extension and rifting. Following this heating event, the lower boundary is returned to 800°C and temperatures diffuse back to the normal conditions over time. We acknowledge that it is unrealistic that temperature would return to a fixed value immediately after this heating event, however, this is sufficient to highlight this process. The background exhumation rate is set to 0.075 km/Ma for the duration of the model. This value is slightly higher than the 0.02 km/Ma inferred using cosmogenic nuclide concentration measurements (Jonell et al., 2017) but we hope to highlight that a constant exhumation rate through time can produce the observed cooling history, and 0.02 km/Ma for the duration of the model would require impossibly high geothermal gradients to exhume rocks from high enough temperatures. This scenario produces a reheating signal as temperatures increase, then as temperatures decrease and rocks continue to exhume, a pulse of cooling is predicted. There is a hint of reheating in the QTQt models. However, it is not very strong and is poorly resolved. Cooling rates during the cooling pulse are lower than in the other two scenarios. However, the geothermal gradient is much higher and decreases through time, as required by the data.

These three scenarios highlight the range of geological models that produce similar time-temperature paths. Other geological models could be envisioned including changing thermal diffusivities through time, different boundary conditions, or many other factors. The large changes in geothermal gradient through time predicted by QTQt are hard to reproduce with a simple advection-diffusion equation and require changes in boundary conditions through time or the emplacement of hot material at the base of the model, as simulated in scenario 3. However, the rate of cooling following this is too slow in scenario 3 and this suggests that there is additional

exhumation during rifting. The data are, therefore, likely providing a record of accelerated erosion during rifting and additional heating possibly related to magmatic underplating in the lower crust.

5.2. Enhanced Denudation Associated With Monsoon Climate?

Climate is a key driver of denudation. The study area is affected by the East Asian monsoon and therefore the changes in cooling rate detected by the thermochronometry might reflect enhanced rates of erosion and exhumation driven by monsoon climate change. Reconstructions of the East Asian monsoon show a relatively stable wet environment throughout the late Eocene and Oligocene that strengthened after 23 Ma, reaching a maximum between 18 and 10 Ma (Clift et al., 2014; Farnsworth et al., 2019). These timings do not coincide with the changes seen in the apatite thermal histories. Notably, cooling rates declined at a time when the monsoon intensified. Hence there is no obvious connection between changes in monsoon intensity and regional thermal history.

In the offshore basins lacustrine/fluvial environments dominated the Eocene, and sediment accumulation rates do not appear to change, although this could be due to limited accommodation space and poor development of regional drainage systems. Between the Oligocene and early Miocene there was a switch from siliciclastic sedimentation to carbonates associated with shallow marine lagoonal and reefal environments. Only in the latest part of the Miocene do offshore basins record a marked rise in siliciclastic sedimentation, largely associated with shoreface facies. At this time accumulation rates were sufficiently high to cause progradation, especially in the Phu Khanh Basin (Fyhn, Nielsen, et al., 2009; Lee et al., 1998). Paradoxically, this occurred at a time when the East Asian monsoon began weakening (Clift et al., 2014). Likewise, ^{10}Be Cosmogenic derived denudation rates for the Song Gianh monsoon-dominated river in northern central Vietnam (Jonell et al., 2017), show lower rates for the strong monsoon of the Early Holocene compared to longer term erosion rates based on local apatite thermochronometry data. Based on this evidence past changes in monsoon climate intensity do not explain the thermochronometry data.

5.3. Timing of Surface Uplift

By the early Cenozoic, it is widely held that a peneplain or low relief surface extended across much of Indochina, hence surface uplift must post-date this. Tighter constraints are provided by the onshore geology. Onshore South Vietnam, the c. 300 km long Song Ba Rift formed within a major NW–SE-trending strike-slip fault zone (Figure 1) that continues offshore and separates the Phu Khanh Basin from the Cuu Long Basin. Structural observations show the faults cross-cut Cretaceous rocks and were therefore active in the Cenozoic when deformation reactivated the strike-slip faults as extensional faults (Nielsen et al., 2007). The Song Ba rift contains up to 500 m of syn-rift Oligocene sediments but their thermal maturity (vitrinite reflectance % Ro c. 0.4) indicates that the grabens were originally deeper and contained more fill, between 1 and 2 km. This means that substantial uplift and denudation occurred after the Oligocene but before eruption of the Miocene basalts that drape the uplift unconformity (Nielsen et al., 2007). Some basalt flows are also seen to infill preexisting valleys. Hoang et al. (2013) provide examples of 6–8 Ma lava flows (their Figure 2) infilling over 300 m of local relief. Such evidence favors a close relationship between topographic growth and rifting although it is possible surface uplift continued after active rifting had ended.

5.4. Paleogene Rifting

The 37–30 Ma interval of accelerated cooling recorded by the thermochronometry data overlaps active rifting in both onshore and offshore basins across central and South Vietnam. Onshore evidence for active erosion during this time can be found within Oligocene clastic deposits of the Di Linh Formation of the Da Lat zone. Detrital zircon U-Pb data from these rocks are dominated by Cretaceous magmatic ages, consistent with erosion of the Cretaceous igneous rocks on which they sit (Hennig et al., 2018). The Di Linh Formation is possibly an extension of the offshore Cuu Long Basin where sediments were first deposited during the latest middle Eocene. Similar to onshore, Paleogene sediments rest on an older basement that includes exhumed Cretaceous granites. Active rifting and inversion took place during the late Eocene to early Oligocene and had almost ceased by the end of the Lower Oligocene, recorded by a basin-wide unconformity dated to c. 28 Ma (Morley et al., 2019). After this the basin entered a short period of compression due to the Mekong Delta Fault Zone switching from left-lateral

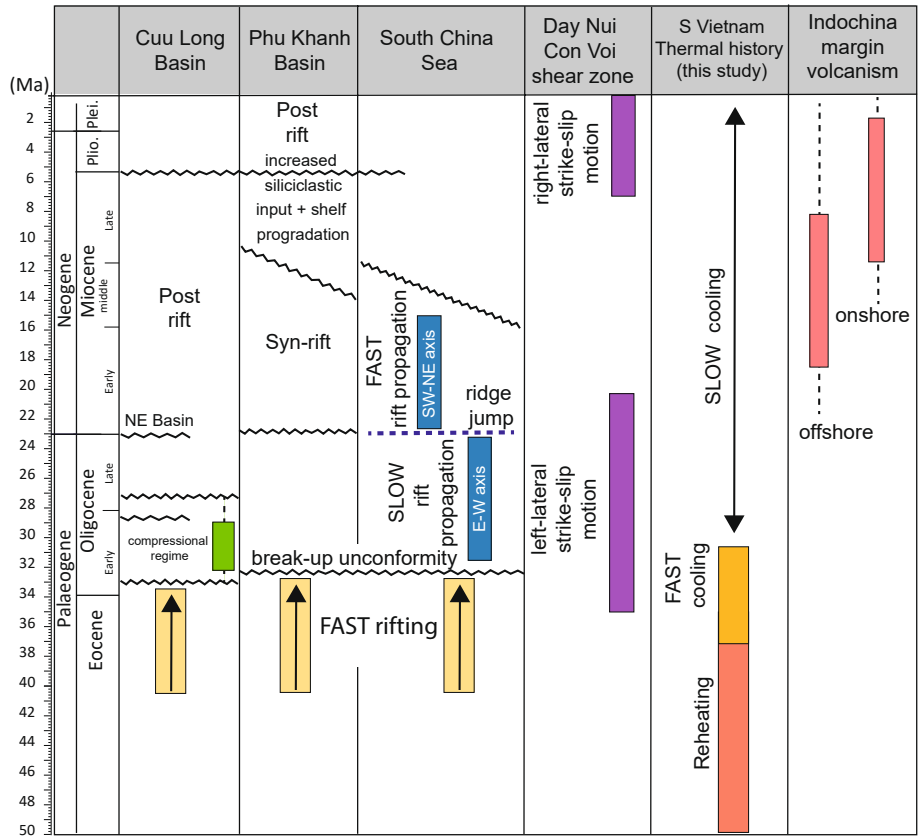

Figure 10. Principal features of the marine basins adjacent to the study area (Fyhn, Boldreel, & Nielsen, 2009; Morley et al., 2019; Schmidt et al., 2019; Vu et al., 2021) compared to the spreading history of the South China Sea (Larsen, 2018; Le Pourhiet et al., 2018), exhumation data, and volcanism across the Indochina margin (Hoang et al., 2013).

to right-lateral strike-slip (Schmidt et al., 2019). This regime ended circa 25 Ma when strike-slip motion on the Mekong Delta Fault Zone stopped, and the basin then transitioned into post rift thermal subsidence.

The influence of a large fault zone is also seen in the Phu Khan Basin where left-lateral motion along the East Vietnam Boundary Fault Zone (Figure 1) affected early rifting (Fyhn, Boldreel, & Nielsen, 2009). Easternmost parts of the basin also show evidence for contemporaneous NW to SE extension suggesting some of the extension was due to other factors, such as slab pull from subduction of a proto-South China Sea (Vu et al., 2021). An unconformity at the Oligocene-Miocene boundary marks the end of rifting in this basin, and a switch to regional post-rift subsidence led to a transgression.

The 37–30 Ma interval of accelerated cooling recorded by the thermochronometry data also spanned regional changes in the stress regime associated with rifting and the onset of ocean spreading c. 32 Ma (Figure 10). Ocean Discovery Program expeditions 367/368, at the northern South China Sea margin, identified a major period of fast extension during the late Eocene to early Oligocene (Larsen, 2018), roughly 40–30 Ma. This relatively short rifting event spanned the rift-to-igneous crustal accretion transition and was associated with rapid upwelling of the asthenosphere, seeding the seafloor spreading that took place soon after. This would have affected all surrounding margins, and it culminated in the formation of a regional breakup unconformity at circa 33–28 Ma after which there was a regional reduction in extensional activity (Morley, 2016, 2019). This timing is shared by basins offshore the study area. During this time Indochina also underwent extrusion along the Ailao Shan-Red River Fault Zone (ARRFZ). Left-lateral shearing along the Day Nui Con Voi shear zone, the southern extension of the ARRFZ, took place between ~35 Ma and ~20 Ma (Jolivet et al., 2001; Leloup et al., 2001; Liu et al., 2020; Searle et al., 2010). However, it seems unlikely that this had a major influence on deformation across the study area since the duration of extrusion extended well beyond the episode of fast cooling.

5.5. Relationship to Ocean Spreading

Onset of seafloor spreading at magnetic anomaly 11, c. 32 Ma (Barckhausen et al., 2014; Sibouet et al., 2016) began in the East South China Sea subbasin opening in a roughly N-S direction. But, at 23 Ma (anomaly 6a) a ridge jump changed the position and direction of spreading by rotating about 15–20° anticlockwise to form the South West subbasin (Sibouet et al., 2016). This shift in orientation caused a change in regional stress and coincides with unconformities in the Cuu Long and Phu Khanh basins (Figures 1 and 8; Fyhn, Boldreel, & Nielsen, 2009; Schmidt et al., 2019). Changes in the regional stress regime are also indicated by changes in rates of the propagation of spreading. Between 32 and 23 Ma rates of propagation in the East South China Sea subbasin were slow but increased in both subbasins after the ridge jump (Le Pourhiet et al., 2018).

Were these changes sufficient to explain the fast cooling? During spreading, as the asthenosphere rises and spreads along the rift axis there will be accompanying changes in the force balance between far-field stresses, resulting from margin composition, structure and topography, and local buoyancy from thinning of the lithosphere. Margin uplift would be expected where the rising asthenosphere induces gradients of gravitational potential energy by juxtaposing denser asthenospheric material against thicker crustal material (Mondy et al., 2018; Rey, 2001), however, a large topographic load from the surrounding continental margin can transmit significant compressive stresses that oppose buoyancy forces. In the case of the South China Sea (East Vietnam Sea) 3D numerical simulations have demonstrated how a small amount of compression, and/or extension, acting normal to the direction of propagation can influence the rate of breakup propagation (Le Pourhiet et al., 2018). The slow propagation stage of rifting within the East South China Sea subbasin can be explained by resistive, compressive stresses from the west-to-east topographic load of Indochina. The change following the ridge jump at 23 Ma, caused the direction of spreading propagation to become oblique to Indochina and reduced much of the resisting out-of-plane compression allowing the propagation of spreading to the SW to accelerate. While the slow propagation stage overlaps with the fast cooling seen in the QTQt models (Figure 6), this is not the case for the timing of the switch to fast rift propagation since it significantly post-dates the slowdown in cooling rates. Thus, while it may be appealing to link the onshore thermal history to changes in spreading and regional stresses there is no strong evidence to support this.

5.6. Relationships to Mantle Structure

Between ~17 and 0.2 Ma widespread intraplate volcanism took place across south-central Vietnam (Hoang et al., 2013) and is effectively ongoing. A common view is that the late Miocene increased siliciclastic sedimentation in basins along the margins of south-central Vietnam was a response to margin surface uplift (Fyhn, Boldreel, & Nielsen, 2009) and that this may have been linked to the widespread basaltic magmatism (Carter et al., 2000). Hoang et al. (2013) observed that the large magmatic centers in Vietnam formed in pull apart basins and that the pattern of volcanism had evolved from SW–NE transtension to E–W extension linked to changes in the lithospheric stress field due to either collision-related lithospheric response or an effect of asthenospheric flow. Using a 1-D shear velocity model for the Indochina block, Yang et al. (2015) identified a low-Vs anomaly below depths of 100 km along South-Central Vietnam and considered it likely reflects active mantle flow in the asthenosphere beneath the region due to the stretching and thinning of the lithosphere. The nature of flow is unclear, however, but could be related to edge-driven convection as this has been used to explain intraplate volcanism and high topography in areas where there is a significant gradient in lithosphere thickness (Kaislaniemi & van Hunen, 2014). While the patterns and consequences of edge-driven convection on the continental side of a passive margin has yet to be fully investigated, it is noted that local conditions for such flow are suitable. The study area has an average crustal thickness between 29 and 33 km (Bai et al., 2009; Vu et al., 2021), thinner than global average values (~36–41 km; Szwillus et al., 2019) and the study area lithospheric thickness is lower, between 110 and 120 km, compared to >130 km for northern Vietnam (Vu et al., 2021). In relation to the apatite thermochronometry results early flow associated with initial thinning and breakup would explain the interval of rapid cooling and account for some of the margin uplift.

An alternative explanation to the above is related to low velocity anomalies detected in the lower mantle below the study area (spanning depths between ~700 and 2,889 km). Using multiscale global tomography Zhao et al. (2021) interpreted the low velocity anomalies below southern Indochina as hot mantle upwellings associated with a cluster of dying or already dead plumes that existed in the Cenozoic. Basalt compositions across the study area are Ocean Island Basalt (OIB) mantle or Enriched Mantle types. An et al. (2017) argued that while there is large-ion

lithophile element enrichment without high field strength element depletion, typical of OIB, NiO -olivine plots show compositions that fall within the range of Hawaiian and Hainan basalt olivines. As these may be produced by partial melting of silica-poor eclogite and peridotite An et al. (2017) favored a Hainan plume source from recycled eclogitic oceanic crust. An alternative explanation for basalt compositions is provided by Hoang et al. (2003) who highlighted the role of active mantle flow in the asthenosphere by arguing that the late Cenozoic alkalic magmatism in East Asia originated in the shallow ductile asthenosphere from adiabatic decompression caused by pronounced changes in stress regimes linked to India-Eurasia collision and subduction of the Pacific Plate. India-Eurasia collision and subduction clearly impacted on mantle structure beneath Indochina as shown by a regional-scale receiver function study of the mantle transition zone discontinuities (Yu et al., 2017). This work highlighted the potential role of the subducted Indian slab and how broken segments sinking into the mantle transition zone could have influenced mantle structure and dynamics beneath the Indochina Peninsula. Clearly further work is needed to fully understand the nature of the magmatism and its relationship to mantle structure.

6. Conclusions

The dense array of apatite thermochronometry results from across and along the margin of south-central Vietnam revealed a regional episode of fast cooling that took place between 37 and 30 Ma. This signal is present along the coastal margin as well as inland. Consideration of the multiple factors that affected the regional stress field at this time highlighted the coincidence between the episode of fast cooling and the period of fast extension across the South China Sea (East Sea) region. This shows a close relationship to rifting. As the episode of cooling might also be due to transient changes in geothermal gradient thermal models explored the relationship between cooling and exhumation. Models rule out thermal relaxation following Mesozoic arc magmatism as geotherms returned to background rates 40–30 Myrs before the onset of fast cooling. Instead, models suggest fast cooling could be attributed to accelerated erosion during early stages of rifting, possibly with some additional heating from either underplating, and/or hot mantle upwellings although the timing does not coincide with known periods of magmatism. No evidence was found to connect regional uplift with the Miocene to Quaternary intraplate magmatism. If this did occur the magnitude of associated surface uplift is beyond the resolution of this study.

Data Availability Statement

Data sets for this research are provided in Tables S1 to S3 in Supporting Information S1. Data are also available on Zenodo at https://zenodo.org/record/5954794#.Yftz3epBxPY.

Acknowledgments
This work has been financially supported by the National Foundation for Science and Technology Development of Vietnam–NAFOSTED (Grant No.: 105.99–2019.302). The authors thank Birkbeck College, University of London, the London Geochronology Centre and Hanoi University of Mining and Geology for access to their analytical and experimental facilities. Our appreciation goes to Michael Fyhn and Lynne Elkins for their constructive reviews and suggestions.

References

An, A.-R., Hi, S., Choi, S. H., Yu, Y., & Lee, D.-C. (2017). Petrogenesis of late cenozoic basaltic rocks from southern Vietnam. *Lithos*, *272–273*, 192–204. https://doi.org/10.1016/j.lithos.2016.12.008

Andersen, C., Mathiesen, A., Nielsen, L. H., Tiem, P. V., Petersen, H. I., & Diem, P. T. (2005). Evaluation of petroleum systems in the northern part of the Cainozoic Song Hong Basin (Gulf of Tonkin), Vietnam. *Journal of Petroleum Geology*, *28*, 167–184. https://doi.org/10.1111/j.1747-5457.2005.tb00078.x

Bai, L., Iidaka, T., Kawakatsu, H., Morita, Y., & Dzung, N. Q. (2009). Upper mantle anisotropy beneath Indochina block and adjacent regions from shear-wave splitting analysis of Vietnam broadband seismograph array data. *Physics of the Earth and Planetary Interiors*, *176*, 33–43. https://doi.org/10.1016/j.pepi.2009.03.008

Barckhausen, U., Engels, M., Franke, D., Ladage, S., & Pubellier, M. (2014). Evolution of the South China Sea: Revised ages for breakup and seafloor spreading. *Marine and Petroleum Geology*, *58*, 599–611. https://doi.org/10.1016/j.marpetgeo.2014.02.022

Carter, A., Roques, D., & Bristow, C. S. (2000). Denudation history of onshore Central Vietnam: Constraints on the cenozoic evolution of the western margin of the South China Sea. *Tectonophysics*, *322*, 265–277. https://doi.org/10.1016/s0040-1951(00)00091-3

Clift, P. D., Brune, S., & Quinteros, J. (2015). Climate changes control offshore crustal structure at South China Sea continental margin. *Earth and Planetary Science Letters*, *420*, 66–72. https://doi.org/10.1016/j.epsl.2015.03.032

Clift, P. D., Wan, S., & Bluszrajn, J. (2014). Reconstructing chemical weathering, physical erosion and monsoon intensity since 25 Ma in the northern South China Sea: A review of competing proxies. *Earth-Science Reviews*, *130*, 86–102. https://doi.org/10.1016/j.earscirev.2014.01.002

Donelick, R. (1993). Apatite etching characteristics versus chemical composition. *Nuclear Tracks and Radiation Measurements*, *21*, 604.

Doust, H., & Sumner, S. H. (2007). Petroleum systems in rift basins–A collective approach in Southeast Asian basins. *Petroleum Geoscience*, *13*, 127–144. https://doi.org/10.1144/1354-079307-746

Farnsworth, A., Lunt, D. J., Robinson, S. A., Valdes, P. J., Roberts, W. H. G., Clift, P. D., et al. (2019). Past East Asian monsoon evolution controlled by paleogeography, not CO_2. *Science Advances*, *5*, eaax1697. https://doi.org/10.1126/sciadv.aax1697

Flower, M., Tamaki, K., & Hoang, N. (1998). Mantle extrusion: A model for dispersed volcanism and DUPAL-like asthenosphere in East Asia and the western Pacific. In M. Flower, S.-L. Chung, C.-H. Lo, & T. Y. Lee (Eds.), *Mantle dynamics and plate interactions in East Asia*, (Vol. 27, pp. 67–88). American Geophysical Union, Geophysical Monograph Series. https://doi.org/10.1029/gd027p0067

Flowers, R. M., Ketcham, R. A., Shuster, D. L., & Farley, K. A. (2009). Apatite (U–Th)/He thermochronometry using a radiation damage accumulation and annealing model. *Geochimica et Cosmochimica Acta*, *73*(8), 2347–2365. https://doi.org/10.1016/j.gca.2009.01.015

Fox, M., & Carter, A. (2020). Heated topics in Thermochronology and paths towards resolution. *Geosciences*, *10*(9), 375. https://doi.org/10.3390/geosciences10090375

Fyhn, M. B. W., Boldreel, L. O., & Nielsen, L. H. (2009a). Geological development of the central and South Vietnamese margin: Implications for the establishment of the South China Sea, indochinese escape tectonics and cenozoic volcanism. *Tectonophysics*, *478*, 184–214. https://doi.org/10.1016/j.tecto.2009.08.002

Fyhn, M. B. W., Nielsen, L. H., Boldreel, L. O., Tahng, L. D., Bojesen-Koefoed, J., et al. (2009). Geological evolution, regional perspectives and hydrocarbon potential of the northwest Phu Khanh Basin, offshore Central Vietnam. *Marine and Petroleum Geology*, *26*, 1–24. https://doi.org/10.1016/j.marpetgeo.2007.07.014

Gallagher, K. (2012). Transdimensional inverse thermal history modelling for quantitative thermochronology. *Journal of Geophysical Research*, *117*(B2), B02408. https://doi.org/10.1029/2011jb008825

Gallagher, K., & Brown, R. (1997). The onshore record of passive margin evolution. *Journal of the Geological Society*, *154*(3), 451–457. https://doi.org/10.1144/gsjgs.154.3.0451

Gautheron, C., Tassan-Got, L., Barbarand, J., & Pagel, M. (2009). Effect of alpha-damage annealing on apatite (U–Th)/He thermochronology. *Chemical Geology*, *266*(3–4), 157–170.

Hall, R. (2012). Late Jurassic-cenozoic reconstructions of the Indonesian region and the Indian ocean. *Tectonophysics*, *570*, 1–41. https://doi.org/10.1016/j.tecto.2012.04.021

Hennig, J., Breitfeld, H., Gough, A., Hall, R., Van Long, T., Mai Kim, V., & Dinh Quang, S. (2018). U-Pb Zircon ages and Provenance of upper cenozoic Sediments from the Da Lat Zone, SE Vietnam: Implications for an intra-miocene unconformity and paleo-drainage of the proto–Mekong River. *Journal of Sedimentary Research*, *88*, 495–515. https://doi.org/10.2110/jsr.2018.26

Hennig-Breitfeld, J., Hennig-Breitfeld, H. T., Sang, D. Q., Vinh, M. K., Long, T. V., Thirwell, M., & Cuong, T. X. (2021). Ages and character of igneous rocks of the Da Lat Zone in SE Vietnam and adjacent offshore regions (Cuu long and Nam Con Son basins). *Journal of Asian Earth Sciences*, *218*, 104878. https://doi.org/10.1016/j.jseaes.2021.104878

Hoang, N., & Flower, M. F. J. (1998). Petrogenesis of cenozoic basalts from Vietnam: Implication for origins of a 'diffuse igneous province. *Journal of Petrology*, *39*, 369–395. https://doi.org/10.1093/petroj/39.3.369

Hoang, N., Flower, M. F. J., Chi, C. T., Xuan, P. T., Quy, H. V., & Son, T. T. (2013). Collision-induced basalt eruptions at Pleiku and Buon Me Thuot, south-central Viet Nam. *Journal of Geodynamics*, *69*, 65–83. https://doi.org/10.1016/j.jog.2012.03.012

Hurford, A. J., & Green, P. F. (1983). The zeta age calibration of fission track dating. *Chemical Geology*, *1*, 285–317. https://doi.org/10.1016/s0009-2541(83)80026-6

Jolivet, L., Beyssac, O., Goffé, B., Avigad, D., Lepvrier, C., Maluski, H., & Thang, T. T. (2001). Oligo-miocene midcrustal subhorizontal shear zone in Indochina. *Tectonics*, *20*, 46–57. https://doi.org/10.1029/2000tc900021

Jonell, T. N., CliftHoang, P. D. L. V., Hoang, T., Carter, A., Wittmann, H., Böning, P., & Rittenour, T. (2017). Controls on erosion patterns and Sediment transport in a monsoonal, Tectonically Quiescent drainage, Song Gianh, central Vietnam. *Basin Research*, *29*, 659–683. https://doi.org/10.1111/bre.12199

Kaislaniemi, L., & Hunen, J. (2014). Dynamics of lithospheric thinning and mantle melting by edge driven convection: Application to Moroccan Atlas mountains. *Geochemistry, Geophysics, Geosystems*, *15*, 3175–3189. https://doi.org/10.1002/2014GC005414

Ketcham, R. A., Carter, A., Donelick, R. A., Barbarand, J., & Hurford, A. J. (2007). Improved modeling of fission-track annealing in apatite. *American Mineralogist*, *92*(5–6), 799–810.

Larsen. (2018). Rapid transition from continental breakup to igneous oceanic crust in the South China Sea. *Nature Geoscience*, *11*, 782–789. https://doi.org/10.1038/s41561-018-0198-1

Lee, G. H., Lee, K., & Watkins, J. S. (2001). Geological evolution of the Cuu long and Nam Con Son Basins, offshore southern Vietnam, South China Sea. *AAPG Bulletin*, *85*, 1055–1082. https://doi.org/10.1306/8626ca69-173b-11d7-8645000102c1865d

Lee, G. H., & Watkins, J. S. (1998). Seismic stratigraphy and hydrocarbon potential of the Phu Khan Basin, offshore central Vietnam, south China Sea. *AAPG Bulletin*, *82*, 1711–1735.

Leloup, P. H., Arnaud, N., Lacassin, R., Kienast, J. R., Harrison, T. M., Phan Trong, T. T., et al. (2001). New constraints on the structure, thermochronology, and timing of the Ailao Shan-Red River shear zone, SE Asia. *Journal of Geophysical Research*, *106*, 6683–6732. https://doi.org/10.1029/2000jb900322

Le Pourhiet, L., Chamot-Rooke, N., Delescluse, M., May, D. A., Watremez, L., & Pubellier, M. (2018). Continental break-up of the South China Sea stalled by far-field compression. *Nature Geoscience*, *11*, 605–609. https://doi.org/10.1038/s41561-018-0178-5

Li, C.-F., Xu, X., Lin, J., Sun, Z., Zhu, J., Yao, Y., et al. (2014). Ages and magnetic structures of the South China Sea constrained by deep tow magnetic surveys and IODP Expedition 349. *Geochemistry, Geophysics, Geosystems*, *15*, 4958–4983. https://doi.org/10.1002/2014gc005567

Li, Y., Abbas, A., Li, C. F., Sun, T., Zlotnik, S., Song, T., et al. (2020). Numerical modeling of failed rifts in the northern South China Sea margin: Implications for continental rifting and breakup. *Journal of Asian Earth Sciences*, *199*, 104402. https://doi.org/10.1016/j.jseaes.2020.104402

Lisker, F., Ventura, B., & Glasmacher, U. A. (2009). Apatite thermochronology in modern geology. *Geological Society, London, Special Publications*, *324*, 1–23. https://doi.org/10.1144/sp324.1

Liu, J. L., Chen, X. Y., Tang, Y., Song, Z. J., & Wang, W. (2020). The Ailao Shan-Red River shear zone revisited: Timing and tectonic implications. *GSA Bulletin*, *132*(5–6), 1165–1182. https://doi.org/10.1130/b35220.1

Luong, T.D., & Bao, N.X. (1988) General Department of Mines and Geology. (1988). *Geological Map of Vietnam, 1:500,000 Scale*. General department of geology and minerals of Vietnam, Hanoi (in Vietnamese).

Matthews, S. J., Fraser, A. J., Lowe, S., Todd, S. P., & Peel, F. J. (1997). Structure, stratigraphy and petroleum geology of the SE Nam Con Son, offshore Vietnam. In A. J. Fraser, S. J. Matthews, & R. W. Murphy (Eds.), *Petroleum geology of southeast Asia*, (Vol. 126, pp. 89–106). Geological Society, London, Special Publication. https://doi.org/10.1144/gsl.sp.1997.126.01.07

Mondy, L. S., Rey, P. F., Ducleaz, G., & Moresi, L. (2018). The role of asthenospheric flow during rift propagation and breakup. *Geology*, *46*, 103–106. https://doi.org/10.1130/g39674.1

Morley, C. K. (2016). Major unconformities/termination of extension events and associated surfaces in the South China Seas: Review and implication for tectonic development. *Journal of Asian Earth Sciences*, *120*, 62–86. https://doi.org/10.1016/j.jseaes.2016.01.013

Morley, R. J., Dung, B. V., Tung, N. T., Kullman, R. J., Bird, R., Van Kieu, et al. (2019). High-resolution Palaeogene sequence stratigraphic framework for the Cuu Long Basin, offshore Vietnam, driven by climate change and tectonics, established from sequence biostratigraphy. *Palaeogeography, Palaeoclimatology, Palaeoecology*, *530*, 113–135. https://doi.org/10.1016/j.palaeo.2019.05.010

Murray, K. E., Braun, J., & Reiners, P. W. (2018). Toward robust interpretation of low-temperature thermochronometers in magmatic terranes. *Geochemistry, Geophysics, Geosystems*, *19*, 3739–3763. https://doi.org/10.1029/2018GC007595

Nguyen, V. V., & Hoai, L. T. T. (2019). Cenozoic paleostress evolution in south central Vietnam: Implication for changing dynamics of faulting along the eastern Indochina continental margin. *Journal of Asian Earth Sciences*, *185*, 104006. https://doi.org/10.1016/j.jseaes.2019.104006

Nielsen, L. H., Petersen, H. I., Thai, N. D., Duc, N. A., Fyhn, M. B. W., Boldreel, L. O., et al. (2007). A middle–upper miocene fluvial–lacustrine rift sequence in the Song Ba Rift, Vietnam: An analogue to oil-prone, small-scale continental rift basins. *Petroleum Geosciences*, *13*, 145–168. https://doi.org/10.1144/1354-079307-748

Pubellier, M., Rangin, C., Le Pichon, X., & Dotsea Working group. (2005). Dotsea: A synthesis of deep marine data in Southeast Asia. *Memoires de la Societe Geologique de France*, *176*, 1–32.

Rangin, C., Huchon, P., Le Pichon, X., Bellon, H., Lepvrier, C., Roques, D., et al. (1995). Cenozoic deformation of central and South Vietnam. *Tectonophysics*, *235*, 179–196. https://doi.org/10.1016/0040-1951(95)00006-2

Rey, P. (2001). From lithospheric thickening and divergent collapse to active continental rifting. In J. A. Miller et al., (Eds.), *Continental reactivation and reworking*, (Vol. 184, pp. 77–88). Geological Society of London Special Publication. https://doi.org/10.1144/gsl.sp.2001.184.01.05

Roques, D., Matthews, S. J., & Rangin, C. (1997). Constraints on strike-slip motion from seismic and gravity data along the Vietnam margin offshore Da Nang: Implications for hydrocarbon prospectivity and opening of the east Vietnam Sea. In A. J. Fraser, S. J. Matthews, & R. W. Murphy (Eds.), *Petroleum geology of southeast Asia*, (Vol. 126, pp. 341–353). Geological Society, London, Special Publication. https://doi.org/10.1144/gsl.sp.1997.126.01.20

Savva, D., Pubellier, M., Franke, D., Chamot-Rooke, N., Meresse, F., Steuer, S., & Auxietre, J. L. (2014). Different expressions of Rifting on the South China Sea margins. *Marine and Petroleum Geology*, *58*, 579e598d. https://doi.org/10.1016/j.marpetgeo.2014.05.023

Schmidt, W. J., Bui, H. H., Handschy, J. W., Vu, T. H., Trinh, X. C., & Nguyen, T. T. (2019). Tectonic evolution and regional setting of the Cuu Long Basin. *Vietnam. Tectonophysics*, *757*, 36–57. https://doi.org/10.1016/j.tecto.2019.03.001

Searle, M. P., Yeh, M. W., Lin, T. H., & Chung, S. L. (2010). Structural constraints on the timing of left-lateral shear along the Red River shear zone in the Ailao Shan and Diancang Shan Ranges, Yunnan, SW China. *Geosphere*, *6*, 316–338. https://doi.org/10.1130/ges00580.1

Shellnutt, J. G., Lan, C.-Y., Long, T. V., Usuki, T., Yang, H.-J., Mertzman, S. A., et al. (2013). Formation of Cretaceous Cordilleran and post-orogenic granites and their microgranular enclaves from the Dalat zone, southern Vietnam: Tectonic implications for the evolution of Southeast Asia. *Lithos*, *182–183*, 229–241. https://doi.org/10.1016/j.lithos.2013.09.016

Sibouet, J.-C., Yeh, Y.-C., & Lee, C.-S. (2016). Geodynamics of the South China Sea. *Tectonophysics*, *692*, 98–119.

Szwillus, W., Afonso, J. C. C., Ebbing, J., & Mooney, W. D. (2019). Global crustal thickness and velocity structure from geostatistical analysis of seismic data. *Journal of Geophysical Research: Solid Earth*, *124*, 1626–1652. https://doi.org/10.1029/2018jb016593

Taylor, B., & Hayes, D. E. (1983). Origin and history of the South China Sea Basin. In D. E. Hayes (Ed.), *The tectonic and geologic evolution of southeast asian seas and islands. Part 2. Geophysical monograph, 27* (pp. 23–56). AGU. https://doi.org/10.1029/gm027p0023

Thuy, N. T. B., Muharren, S., Wolfgang, S., & Fukun, C. (2004). Granitoids in the Dalat zone, Southern Vietnam: Age constraints on magmatism and regional geological implications. *International Journal of Earth Sciences*, *93*, 329–340.

Vu, A. T., Fyhn, M. B. W., Xuan, C. T., Nguyen, T. T., Hoag, D. N., Pham, L. T., & Van, H. N. (2021). Cenozoic tectonic and stratigraphic development of the Central Vietnamese continental margin. *Marine and Petroleum Geology*, *86*, 386–410.

Wildman, M., Cogné, N., & Beucher, R. (2019). Fission-track thermochronology applied to the evolution of passive continental margins. In M. Malusà, & P. Fitzgerald (Eds.), *Fission-track thermochronology and its application to geology*. Springer Textbooks in Earth Sciences, Geography and EnvironmentSpringer. https://doi.org/10.1007/978-3-319-89421-8_20

Yang, Y., Liu, F., Harmon, N., Phon Le, K. O., Gu, S., & Xue, M. (2015). Lithospheric structure beneath Indochina block from Rayleigh wave phase velocity tomography. *Geophysical Journal International*, *200*, 1582–1595. https://doi.org/10.1093/gji/ggu488

Yu, Y., Gao, S. S., Liu, K. H., Yang, T., Xue, M., & Phon Le, K. (2017). Mantle transition zone discontinuities beneath the Indochina Peninsula: Implications for slab subduction and mantle upwelling. *Geophysical Research Letters*, *44*, 7159–7167. https://doi.org/10.1002/2017GL073528

Zhao, D., Toyokuni, G., & Kurata, K. (2021). Deep mantle structure and origin of cenozoic intraplate volcanoes in Indochina, Hainan and South China Sea. *Geophysical Journal International*, *225*, 572–588. https://doi.org/10.1093/gji/ggaa605

Zhu, B.-Q., Wang, H.-F., Chen, Y.-W., Chang, X.-Y., Hu, Y.-G., & Xie, J. (2004). Geochronological and geochemical constraint on the Cenozoic extension of Cathaysian lithosphere and tectonic evolution of the border sea basins in East Asia. *Journal of Asian Earth Sciences*, *24*(2), 163–175.

References From the Supporting Information

Galbraith, R. F., & Laslett, G. M. (1993). Statistical models for mixed fission track ages. *Nuclear Tracks and Radiation Measurements*, *21*, 459–470. https://doi.org/10.1016/1359-0189(93)90185-c

Hurford, A. J. (1990). Standardization of fission track dating calibration: Recommendation by the fission track working Group of the IUGS subcommission on geochronology. *Chemical Geology*, *80*, 177–178. https://doi.org/10.1016/0168-9622(90)90025-8